

Digitized Circular Arcs: Characterization and Parameter Estimation

Marcel Worring and Arnold W.M. Smeulders

Abstract—The digitization of a circular arc causes an inherent loss of geometrical information. Arcs with slightly different local curvature or position may lead to exactly the same digital pattern. In this paper we give a characterization of all centers and radii of circular arcs yielding the same digitization pattern. The radius of the arcs varies over the set. However, only one curvature or radius estimate can be assigned to the digital pattern. We derive an optimal estimator and give expressions for the bound on the precision of estimation. This bound due to digitization is the deterministic equivalent of the Cramér/Rao bound known from parameter estimation theory.

Consider the estimation of the local curvature and local radius of a smooth object. Typically such parameters are estimated by moving a window along the digital boundary. Methods in literature show a poor precision in estimating curvature values, relative errors of over 40% are often found [34]. From the definition of curvature it follows that locally the curve can be considered a circular arc and hence the method presented in this paper can be applied to the pattern in the window giving estimates with optimal precision and a measure for the remaining error.

On the practical side we present examples of the residual error due to the discrete grid. The estimation of the radius or curvature of a circular arc at random position with an estimation window containing 10 points (coded with nine Freemancodes) has a relative deviation exceeding 2%. For a full disk the deviation is below 1% when the radius r exceeds four grid units.

The presented method is particularly useful for problems where some prior knowledge on the distribution of radii is known and where there is a noise-free sampling.

Index Terms—Circular arcs, parameter estimation, curvature, precision, digitization.

I. INTRODUCTION

IN this paper we consider the estimation of geometric features of smooth continuous objects when digitized on a regular grid.

We rely on the fundamental theorem in the differential geometry of curves [28] to find what features are of importance in the analysis of smooth boundary curves. The theorem states that one can reconstruct any smooth curve up to a rigid transformation if curvature is known as function of arc length, where curvature is the inverse of the radius of the circle locally coinciding with the curve. This makes curvature (or the radius of the circular arc for that matter) and arc length the two basic features to consider in the analysis of any smooth (line) figure.

For the estimation of the curvature of the digitized boundary, five essentially different methods are found in [1], [2], [9], [20], [29]. These five methods were compared in [33], [34] on the basis of their performance in measuring the curvature of circular arcs repeatedly placed on a random position with respect to the digitization grid. It turned out that none of the methods yields accurate and precise estimates of curvature.

A theoretical analysis of the methods revealed a number of clues for the poor performance. In [20] the curvature is estimated by applying a linear differentiating filter to the x - and y -coordinate separately. For circular arcs this separation, bypassing the 2D nature of the problem, introduces significant errors due to the truncation of the filter. The methods in [1], [2], [9] find curvature by applying a linear differentiating filter to the estimated orientation. The method in [9] is the only method which explicitly takes the anisotropy of the grid into account and in fact with proper scaling this is the method with best performance. In the other cases errors in the order of 40% are common.

Fitting a circular arc to the digital data does take the two dimensional shape of the digital boundary into account, and algorithms can be found in [4], [18], [29]. It turned out that for noise free digitized circular arcs the precision is poor.

Clearly, the precision of the estimation is limited as a consequence of both the stochastic noise introduced in the imaging system and by the digitization noise. There is, however, an important difference in the characteristics of the two types of noise. Stochastic noise is a random process, and the precision of measurement is limited by the Minimum Variance or Cramér/Rao bound [5]. In contrast, the digitization noise is *not* a random process. It is completely governed by the position and shape of the object and by the deterministic characteristics of the spatial quantization, dependent on the resolution and connectivity of the digitization grid. Hence, for digitization there is a deterministic bound on the precision equivalent to the Cramér/Rao bound. With high precision scanning systems as flat bed scanners or when images are recorded at limited resolution, the stochastic noise is in general much smaller than the digitization noise. For the purpose of accurate measurement this makes the effect of digitization most important. This will, therefore, be the focus of this paper.

Extensive studies on the effect of spatial quantization on straight boundaries [6], [14], [19] led to accurate estimators for measuring arc length and bounds on their precision [7], [8], [16], [17], [24]. These studies also led to very accurate registration of straight digitized boundaries in an image pair [3]. We proceed along the same path as [6], [14], [19] for the analysis of curved boundaries and seek expressions for the deterministic equivalent of the Cramér/Rao bound in local

Manuscript received April 5, 1993.

M. Worring and A.W.M. Smeulders are with the Department of Computer Science, University of Amsterdam, Kruislaan 403, 1098 SJ Amsterdam, The Netherlands; e-mail: worring@fwi.uva.nl; smeulder@fwi.uva.nl.

IEEECS Log Number P95079.

shape estimation as well as a method reaching this bound.

To introduce the concept consider the curvature of a set of points in a window on the digital contour resulting from digitizing the contour of a smooth object. The interest is not in the curvature of the digital pattern, but in the curvature of the preimage of the contour. The digitization causes an inherent loss of geometrical information. Other arcs (with slightly different local curvature or position) may lead to exactly the same digital pattern. Thus, the precision of estimation is limited by the capability of the digital pattern to discriminate small variations in the curvature of the arc. Here we are concerned with the ultimate precision one can reach.

The first step in the analysis is to verify that the digital pattern indeed is the digitization of some circular preimage. Algorithms for this step are presented in [15], [21], [22]. One step further beyond the recognition is to render all centers of circular arcs which generate this pattern [10], not considering the radius of the arc. A complete characterization of all centers and radii is presented in [32]. This is done in [30] also, for a few very simple digital patterns only, using the theory of locales of an object [13]. The theory of locales is not applicable if only part of the boundary of the object is given.

We start off in Section II with an analysis of the digitization process and give a type classification of all possible point sets of limited size. From there the full characterization of digitized circles for a given pattern is studied based on the results in [32]. From there (Section III) we will find expressions for the bound on precision and present an optimal shape parameter estimator for noise free digitized circular arcs. A very preliminary presentation of the concept was presented in [27]. Finally, in Section IV practical bounds are calculated

II. DIGITIZATION AND DOMAINS

A. Digitization

In this section we make precise how the digitization affects a curved object boundary.

For the digitization of an object X we can consider two different digitization models, Grid Intersect Quantization (GIQ) or Object Boundary Quantization (OBQ) [12]. GIQ is appropriate for the generation of arcs in computer graphics, for image processing OBQ is the more common model. Thus we consider OBQ only; the results derived here, however, are applicable for GIQ with minor modifications. We further restrict our attention to eight-connected grids, but this is also a choice not affecting the general idea in the paper; similar results are obtained for four- or six-connected grids.

For eight-connected objects pixels are on the boundary of the digital object if they are four-connected to a pixel in the background. The eight-connected contour of the object X is hence given by:

DEFINITION 1. (*Object Boundary Quantization*)

$$D_{OBQ}(X) = \{s \in \mathbb{Z}^2 \mid s \in X \wedge \exists s' \in N_4(s) : s' \notin X\},$$

where $N_4(s)$ is the set of points four-connected to s . We can order the points of $D_{OBQ}(X)$ in counterclockwise fashion [25].

So we write $D_{OBQ}(X) = \{s_k\}_{k=0, \dots, m-1}$, where m is the number of contour points in X and s_0 an arbitrary starting point.

In the practice of curvature or radius estimation a window of size n' is moved along the points of $D_{OBQ}(X)$, and from this set of points local estimates are derived (see Fig. 1(a) where $n' = 6$). The set of n' points starting at point s_k is defined by:

$$S_p(X, k, n') = \{s_j \in D_{OBQ}(X)\}_{j=k, \dots, ((k+n'-1) \bmod m)}, \quad (1)$$

where the modulo operator is used because we are dealing with closed, and therefore periodic, contours.

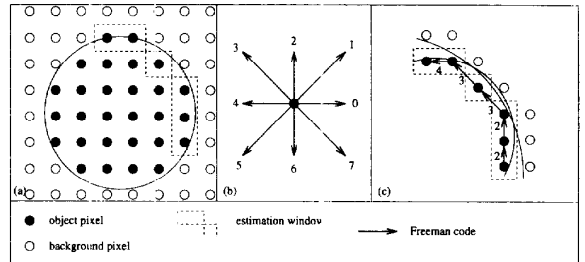


Fig. 1. (a) An original disk X with its object and background pixels. An example estimation window defining the point set S_p is also indicated. (b) Freeman coding of the eight neighbors of a digital point. (c) Coding of the points of S_p using Freeman codes. An alternative circular arc is also given which in the estimation window would lead to exactly the same digital pattern.

The points of the pattern S_p are the points just to the inside of the continuous boundary of X (Definition 1). These points have at least one four-connected neighbor not in S_p . The set S_Q of such associated background pixels is given by:

$$S_Q(S_p) = \{s \in \mathbb{Z}^2 \mid s \notin X \wedge \exists s' \in S_p : s' \in N_4(s)\}. \quad (2)$$

In the sequel we will omit the parameters of S_p and S_Q . The ordered pair of point sets (S_p, S_Q) together constitutes the digital pattern S .

The points of S_p are described using Freeman codes [11]. For each point $s_i \in S_p$, the Freeman code f_i indicates which of the eight possible neighbors of s_i is the next point in S_p (see Fig. 1). Note that the Freeman code is the coding of a vector. The vector (not its coding) is denoted by $\mathbf{v}(f_i)$, where $f_i \in [0, 7]$. The sequence $\{f_i\}_{i=0, n-1}$ with given starting point s_k and $n = n' - 1$, is called the Freeman chain and denoted by F_n . Later we need the forward difference $\Delta f_i = f_{i+1} - f_i$, defined for $i \leq n - 2$. The forward difference is taken modulo 8 in such a way that $\Delta f_i \in [-3, 4]$.

To generate all valid Freeman chains of given length n , and hence all valid sets S_p with $n + 1$ points, which might occur in the digitization of some circular arc, we consider the contour tracing algorithm as defined in [25]. Starting from a contour point $s_0 \in X$ for which $s_0 + \mathbf{v}(0) \notin X$ this algorithm considers neighbors of s_0 in counterclockwise order, starting from $s_0 + \mathbf{v}(0)$, until it encounters another element in X . Then the algorithm continues with this new element in X found and the previous pixel encountered which consequently is not in X .

From the definition of the tracing algorithm it follows that for any point $s_i \in S_p$, with associated Freeman code f_i , the point

$s_i + \mathbf{v}(f_i - 1)$ must be an element of S_Q . Furthermore, if f_i is even, the point $s_i + \mathbf{v}(f_i - 2)$ must also be in S_Q , as otherwise the tracing algorithm would have chosen this point as the next contour point instead of $s_i + \mathbf{v}(f_i)$.

In the digitization of an arbitrary object a Freemancode f_i could be followed by a Freemancode in exactly the opposite direction, i.e., $\Delta f_i = 4$. However, the resulting pattern, (S_P, S_Q) can never be part of the digitization of a circular arc, which is easily verified using the results in Section II.B.

For all the remaining cases we can give one continuous arc (using window size $n = 2$) which has the resulting pattern (S_P, S_Q) as its digitization. Consequently, the possible Freeman differences which can occur in the digitization of a circular arc are given by:

$$\Delta f_i \in \begin{cases} [-1, \dots, 3] & (f_i \in \{0, 2, 4, 6\}) \\ [-2, \dots, 3] & (f_i \in \{1, 3, 5, 7\}) \end{cases} \quad (3)$$

By looking at all points not in the object X which the algorithm considers for an element $s_i \in S_P$ and keeping only those points which are four-connected to a point in S_P we find that the background points q_i associated with s_i are given by:

$$q_i = \begin{cases} \{s_{i+1} + \bigcup_{j=2,3} \mathbf{v}(f_i - j)\} & (f_i \in \{0, 2, 4, 6\} \wedge \Delta f_i \neq 2) \\ \{s_{i+1} + \bigcup_{j=0,2,3} \mathbf{v}(f_i - j)\} & (f_i \in \{0, 2, 4, 6\} \wedge \Delta f_i = 2) \\ \{s_{i+1} + \bigcup_{j=3} \mathbf{v}(f_i - j)\} & (f_i \in \{1, 3, 5, 7\} \wedge \Delta f_i \neq 2) \\ \{s_{i+1} + \bigcup_{j=1,3} \mathbf{v}(f_i - j)\} & (f_i \in \{1, 3, 5, 7\} \wedge \Delta f_i = 2) \end{cases} \quad (4)$$

and finally,

$$S_Q = \bigcap_i q_i. \quad (5)$$

The generation of the patterns is exemplified in Fig. 2.

As there is a direct mapping from a Freemanchain F to the corresponding digital pattern (S_P, S_Q) we will not make a distinction between the two in the sequel and will use the appropriate format to describe the pattern.

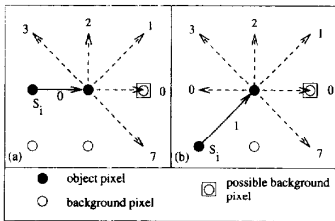


Fig. 2. (a) In an eight-connected boundary five different codes can follow Freemancode 0 originating at s_i . Due to the counterclockwise tracing of the contour an a-symmetric solution is found as the contour code 6 cannot follow code 0 because the code sequence 06 would be replaced by one code 7. Points identified as background pixels (i.e., elements of S_Q) associated with f_i are also shown. For $f_{i+1} = 3$ there is one more background pixel associated with f_i . In the other cases this point is either not part of S_Q ($f_i \in \{0, 7\}$) or is associated with f_{i+1} ($f_i \in \{1, 2\}$); (b) The six codes to follow an odd code with the one associated background pixel. The same special case for $f_{i+1} = 3$ occurs.

B. The Domain of Digitized Circular Arcs

In the previous section we considered the generation of patterns $S = (S_P, S_Q)$. Now we consider the continuous arcs which could have led to a specific digital pattern.

The disk B and its closed complement B^* are given by:

DEFINITION 2. (Circular Disk)

$$B(m, r) = \{c \in \mathbb{R}^2 \mid d(m, c) \leq r\}$$

$$B^*(m, r) = \{c \in \mathbb{R}^2 \mid d(m, c) \geq r\}$$

The 3D-parameter space (m_x, m_y, r) of all centers and radii of arcs is denoted by Ω .

The digitization operator D_{OBQ} (Definition 1) maps elements from the *continuous* space Ω into a pattern in the *discrete* space \mathbb{Z}^2 . A continuum of various (but closely related) arcs $\omega \in \Omega$ are indistinguishable after digitization. Hence, there exists no inverse operator. Now, let (S_P, S_Q) be the pattern corresponding to an estimation window, positioned somewhere along the digital boundary resulting from digitizing disk $B(\omega_0)$. The domain of S is the set of all arcs, which after digitization generate the pattern S somewhere in their digital boundary. To that end we define the domain operator \mathcal{B} , being the pseudoinverse of the digitization operator. It gives the equivalence class of ω_0 :

DEFINITION 3. (Domain Operator)

$$\mathcal{B}(S_P, S_Q) = \{\omega \in \Omega \mid S_P \subset D_{OBQ}(B(\omega))\}.$$

To find the set of all preimages of circular arcs leading to the digital pattern S we need some of the results of [32]. The domain (Definition 3) is given by:

$$\mathcal{B}(S_P, S_Q) = \{(m, r) \in \Omega \mid S_P \subset B(m, r) \wedge S_Q \subset B^*(m, r)\}. \quad (6)$$

Note that, without loss of generality, we include the elements on the boundary of the arc domain as well, although those arcs touch an element in S_Q .

The set of all centers m' such that there exists some radius r' with (m', r') in the arc domain, i.e., the projection of \mathcal{B} onto the 2D-plane, is the generalized Voronoi polygon $V(S_P, S_Q)$ [10], [23]:

$$V(S_P, S_Q) = \{x \mid \forall p \in S_P, q \in S_Q : d(x, p) \leq d(x, q)\}. \quad (7)$$

The region $V(p, q)$, where p and q are elements of S_P and S_Q , is the halfplane containing p and bounded by the perpendicular bisector of (p, q) . It immediately follows that $V(S_P, S_Q)$ can be rewritten into:

$$V(S_P, S_Q) = \bigcap_{p \in S_P, q \in S_Q} V(p, q), \quad (8)$$

showing that $V(S_P, S_Q)$ is a filled (possibly unbounded) convex polygon. In Fig. 3, $V(S_P, S_Q)$ is shown for an example configuration of S_P and S_Q .

For later use, note that the generalized Voronoi polygon generalizes the more familiar closest point Voronoi polygon associated with $s \in S$ which is given by:

$$V(s, S) = \{x \mid \forall s' \in S : d(x, s) \leq d(x, s')\}.$$

In an analogous way, the furthest point Voronoi polygon associated with $s \in S$ is given by:

$$V(S, s) = \{x \mid \forall s' \in S : d(x, s') \geq d(x, s)\}.$$

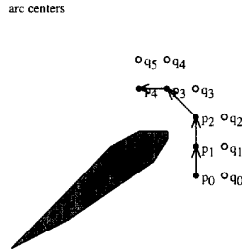


Fig. 3. The pattern S comprised of sets S_p (black dots) and S_q (open dots) with the corresponding Freemanchain of four codes. The generalized Voronoi polygon $V(S_p, S_q)$ (grey) is the set of all centers m such that there exists a radius r' with disk (m, r') including all points of S_p and excluding all of S_q , i.e., (m, r') is in the arc domain. The small area indicated within $V(S_p, S_q)$ is the curved polygon containing all centers m for some fixed radius r_0 . The generalized Voronoi polygon is the union of such regions for varying r .

With (8) we have formulated the set of centers of all pre-image arcs which generate the digital pattern. Before we proceed with the characterization of the domain of centers and radii in Section II.D we distinguish a number of different domain types based on the set of centers only and use it to derive a bound on the radii of arcs which can be analyzed on the basis of a point set described by a Freemanchain of length n .

C. Characterization of Domain Type

In the preceding section we investigated a pattern (S_p, S_q) and found disks including all of S_p and excluding all of S_q locally assuming a convex object. However, when estimating the curvature of an arbitrary smooth object, moving an estimation window along the digital boundary, the original curve can locally either be convex or concave. In the latter case (7) can still be applied, but with the roles of S_p and S_q reversed.

As in general it is not known beforehand which case applies both have to be considered. Depending on whether the domains for the two cases are empty or nonempty four different types are distinguished. For each nonempty domain we consider r_{max} , the radius of the largest disk, which might be finite or infinite. This leads to two more types of patterns (see Fig. 4).

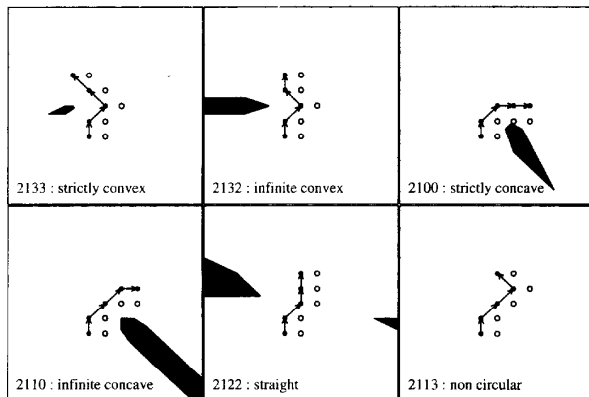


Fig. 4. Examples of patterns corresponding to chains of $n = 4$ codes.

The digital pattern is called straight if both $\mathcal{B}(S_p, S_q) \neq \emptyset$ and $\mathcal{B}(S_q, S_p) \neq \emptyset$. Such patterns should be analyzed as straight lines [6]. When both domains are empty the pattern is called noncircular as no circular arcs exist leading to the given pattern. In the other cases one of the two domains is nonempty. When $\mathcal{B}(S_p, S_q)$ is the nonempty domain the digital pattern is called strictly convex if $r_{max} \neq \infty$ and infinite convex otherwise. Strictly concave and infinite concave are defined likewise.

The different types of patterns are related in the sense that by addition of one Freemancode to a Freemanchain of n codes only a limited number of type changes occur, following directly from the fact that the domain for the Freemanchain with $n + 1$ codes is a subset of the domain of the smaller chain. The possible changes are summarized in Fig. 5.

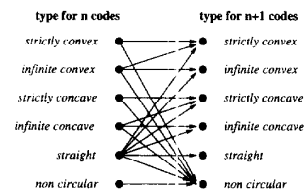


Fig. 5. The limited number of admissible type transitions when a new Freemancode is added to a chain of n codes.

These relations are used in conjunction with (3) to efficiently find all patterns in the set of all Freemanchains of length n (denoted by \mathcal{F}^n) which can be in the digitization of a circular arc. Without loss of generality we limit ourselves to patterns starting with Freemancode 0 or 1. Patterns which are self-intersecting are classified as noncircular as the tracing algorithm discussed in Section II will never generate such patterns. For the same reason patterns with partial overlap are classified noncircular, except when the last point of the pattern equals the first point of the pattern indicating a closed boundary. Counting the number of different types found yields the type classification in Table I.

TABLE I
COUNTING THE TYPE OF ALL $2 \times 8^{n-1}$ FREEMANCHAINS OF LENGTH n WITH 0 OR 1 AS FIRST CODE, THE CLASSIFICATION OF THE PATTERNS IS GIVEN. ALSO GIVEN IS THE MAXIMUM RECOGNIZABLE RADIUS FOR VARYING n , WHERE FOR CONCAVE PATTERNS THE OBVIOUS EXTENSION OF MRR TO SUCH PATTERNS IS USED.

n	type of the pattern							
	convex			concave		straight	non-circular	
	strict	infinite	MRR(n)	strict	infinite			MRR(n)
3	10	6	1.4	5	4	0.5	14	89
4	56	14	2.0	24	11	1.0	26	893
5	171	24	2.6	80	20	1.6	46	7,851
6	399	42	3.3	210	37	2.5	70	64,778
7	821	62	4.0	457	56	3.5	106	522,786
8	1,506	90	5.0	888	83	5.0	150	4,191,587
9	2,575	124	6.0	1,612	116	6.0	206	33,549,799

It follows from the table that only a small fraction of elements in \mathcal{F}^n lead to valid circular patterns. Furthermore, most of these circular patterns are either strictly convex or strictly concave.

Now, consider a continuous disk placed on an arbitrary position with respect to the grid. When moving a window along the digital contour of the disk we expect to find strictly

convex patterns only. However, when the window size is chosen too small the local pattern might be of the infinite convex or even straight type. This is undesirable and poses a limit on the radius of continuous circular arcs we can analyze with a given window size. To be precise, for a window with corresponding Freemanchains of size n the maximum recognizable radius $MRR(n)$ is defined as the radius of the largest disk which at an arbitrary position is assured to yield convex-type patterns only. To find MRR we have to consider all straight and infinite convex patterns corresponding to chains in \mathcal{F}^n and make sure that the radius of the original disk is smaller than the smallest radius in any such domain i.e.,:

DEFINITION 4. (*Maximum Recognizable Radius*)

$$MRR(n) = \min_{F \in \mathcal{F}^n : \text{type}(F) \in \{\text{infinite convex, straight}\}} \{r_{\min}(F)\},$$

where $r_{\min}(F)$ is the minimum radius of any disk in the domain of the pattern associated with F .

In Table I the maximum recognizable radius is given for $n = 3, \dots, 9$. The MRR values show that only small radii can be recognized if the number of codes is limited. For larger n the $MRR(n)$ tends to a linear relationship with n .

D. Characterization of the Arc Domain

In Section II.B the set of all centers of circular arcs which could lead to the given pattern S was shown to be the generalized Voronoi polygon. In this section we consider the full extent of the domain in Ω and present an algorithm for computing a characterization of the domain. As the emphasis in this paper is on the shape estimation part of the problem proofs concerning the characterization will be omitted. Here we give a summary only; interested readers are referred to [32]. We restrict ourselves to the convex case. However, results are exactly the same if the roles of S_P and S_Q are reversed throughout this section. In fact, S_P and S_Q can be two arbitrary disjunct point sets, they do not even have to be confined to the discrete grid.

Now, consider the set of centers for a fixed value of r , denoted by $M_r(S_P, S_Q)$, which consequently is a subset of the generalized Voronoi polygon. This set is given by:

DEFINITION 5. (*Arc Centers*)

$$M_r(S_P, S_Q) = \{m \in \mathbb{R}^2 \mid S_P \subset B(m, r) \wedge S_Q \subset B^*(m, r)\}.$$

Thus, the set of centers is bounded by a polygon with convex and concave edges in its boundary.¹ For an example see Fig. 3. Clearly we have:

$$\bigcup_r M_r(S_P, S_Q) = V(S_P, S_Q) \quad (9)$$

The curved edges in the boundary of $M_r(S)$ form a sequence, where each curved edge is centered at some element in S . They are the points of the set which constitute the local constraint on M_r . Hence, we have an ordering of the elements in S which is denoted by $SEQ_r(S)$.

DEFINITION 6. (*r-sequence*)

$SEQ_r(S)$ = ordered sequence of the elements of S , corresponding to the ordered sequence of edges in $\partial M_r(S)$.

For example, in Fig. 3 we have $SEQ_r(S) = p_2, p_3, q_0, q_1, q_3, q_5$. It should be noted that the r -sequence may actually contain a number of sequences each of which has a cyclic ordering. Further, note that not necessarily every element of S is part of the sequence. The remaining points of S do not play a limiting role on the arcs of radius r .

Every three subsequent points (s', s, s'') in the sequence define one curved edge in the boundary of $M_r(S)$. The point s defines the center of the edge and the points s' and s'' in conjunction with s determine the endpoints of the edge. Whether the edge is convex or concave depends on whether $s \in S_P$ (convex) or $s \in S_Q$ (concave).

For varying r , the shape of ∂M_r changes in a continuous fashion in the sense that the radius of the bounding edges increases. The composition of ∂M_r , i.e., $SEQ_r(S)$ changes only at discrete values of r . At these values of r a new edge is added to the boundary or an existing edge will no longer participate for larger radii. The domain of a pattern S is fully characterized if all changes to $SEQ_r(S)$ are known for varying r .

To compute the characterization we divide $V(S_P, S_Q)$ in regions (in 2D-parameter space) such that every region is critically determined by a specific $s \in S$. For the elements of S_P we use the intersection of the furthest point Voronoi polygon, a structure well known in computational geometry [23], with $V(S_P, S_Q)$. For elements in S_Q we use the closest point Voronoi polygon.

DEFINITION 7. (*s-Region*)

$$L(s) = \begin{cases} V(S_P, s) \cap V(S_P, S_Q) & (s \in S_P) \\ V(s, S_Q) \cap V(S_P, S_Q) & (s \in S_Q) \end{cases}$$

In Fig. 6. the s -regions are shown for a simple arbitrary pattern.

The s -regions provide a disjunct covering of $V(S_P, S_Q)$, which will be called the L_P -diagram for set S_P and the L_Q -diagram for set S_Q .

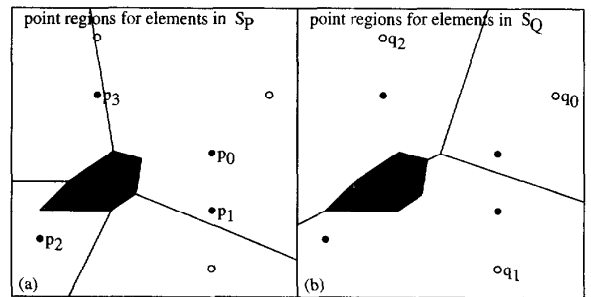


Fig. 6. For every element of $p \in S_P$ the intersection of the generalized Voronoi polygon of S with the furthest point Voronoi polygon corresponding to p yields the s -region of p . For p_1 the corresponding s -region is highlighted (a). In a similar way (b) shows the s -regions of elements in S_Q with the q -region of q_1 highlighted.

1. This should not be confused with the digital pattern being convex or concave. If the digital pattern is concave the roles of S_P and S_Q are reversed, but in the boundary of $M_r(S_Q, S_P)$ still alternating sequences of convex and concave edges are found.

Changes in the r -sequence are related to straight edges and vertices in the two diagrams. To that end we list all admissible transitions of the r -sequence, when increasing r (see Table II). For reasons of simplicity we make the assumption, common in Voronoi related results, that no four points in the pattern S are co-circular.

TABLE II

THIS TABLE GIVES A CHARACTERIZATION OF ALL POSSIBLE ISOLATED CHANGES TO $SEQ_r(S)$ OCCURRING, WHEN r PASSES THROUGH ONE OF THE VALUES IN THE ARC SPECTRUM OF S . THE CHANGE IS DETERMINED BY THE CONFIGURATION OF THE POINTS DEFINING THE MINIMUM OR MAXIMUM DISTANCE TO AN EDGE IN THE L_P - OR L_Q -DIAGRAM DEPENDING ON THE SET(S) THE ELEMENTS STEM FROM AND ON THE TYPE OF TRIANGLE THEY FORM. THE SYMBOLS α AND γ DENOTE A (POSSIBLY) EMPTY SEQUENCE OF POINTS FROM S .

THE CHANGE OCCURS IF r PASSES THROUGH $\rho(T)$, THE RADIUS OF THE SMALLEST DISK CONTAINING T . EVERY ESSENTIALLY DIFFERENT CHANGE IS GIVEN A UNIQUE LABEL. NOTE THAT CASES WHICH ONLY DIFFER IN A REFLECTION OF THE POINTS ARE GIVEN THE SAME LABEL. FURTHER, NOTE THAT IF CASE 14 APPLIES, THE CONTOUR SPLITS INTO TWO SEPARATE COMPONENTS.

configuration		SEQ _r (S)		case
type	point set T	$r = \rho(T) - \epsilon$	$r = \rho(T) + \epsilon$	
obtuse triangle	(p', p, p'')	α, p', p'', γ	$\alpha, p', p, p'' \gamma$	1
	(p', p, q)	α, q, p', p, γ	α, q, p, γ	2
	(q, p, p')	α, p, p', q, γ	α, p, q, γ	
	(p, q, p')	\emptyset	p', q, p	3
	(q, p, q')	q', p, q	\emptyset	4
	(p, q, q')	α, q, p, γ	α, q, q', p, γ	5
	(q', q, p)	α, p, q, γ	α, p, q', q, γ	
	(q', q, q'')	$\alpha, q', q, q'', \gamma$	α, q', q'', γ	6
acute triangle	(p', p, p'')	\emptyset	p', p, p''	7
	(p', p, q)	α, p', p, γ	α, p', q, p, γ	8
	(q, p', p)			
	(p, q, p')			
	(p, q, q')	α, q, p, q', γ	α, q, q', γ	9
	(q, q', p)			
	(q', p, q)			
	(q', q, q'')	q', q, q''	\emptyset	10
right triangle	(p', p, p'')	\emptyset	p', p, p''	7
	(p', p, q)	α, p', p, γ	α, q, p, γ	11
	(q, p, p')	α, p, p', γ	α, p, q, γ	
	(p, q, p')	\emptyset	p', q, p	3
	(q, p, q')	q', p, q	\emptyset	4
	(p, q, q')	α, q, p, γ	α, q, q', p, γ	5
	(q', q, p)	α, p, q, γ	α, p, q', q, γ	
	(q', q, q'')	$\alpha, q', q, q'', \gamma$	α, q', q'', γ	6
minimal distance point pair	(p, p')	\emptyset	p, p'	12
	(p, q)	α, p, γ	α, p, q, p, γ	13
	(q, p)			
	(q, q')	q, α, q', γ	q, q', γ	q', q, α

This table and the L_P - and L_Q -diagrams form the basis for the algorithm to compute the characterization of a pattern S . The pseudocode for this algorithm is given in Fig. 7.

The algorithm first constructs the L_P - and L_Q -diagram. From there the edges in the diagram are assigned a direction, such that the distance to the points of which the edge is the perpendicular bisector is increasing. Edges which properly contain the point of minimum distance cannot be assigned such a direction and therefore such edges are split into two separate edges by introduction of an artificial vertex at the point of minimum distance. Thus, following an edge in its given direction is always corresponding to increasing r .

Recursively all vertices of the diagrams are treated, starting from the vertex defining the minimal disk. At every vertex with all incoming edges labeled, the change to the sequence of

edges in $\partial M_r(S)$ is applied, (where the actual change is determined from Table II) and then the algorithm has to choose the appropriate diagram to continue with. If the vertex considered lies in the interior of $V(S_p, S_q)$ the same diagram has to be chosen. However, if the vertex lies on the boundary of $V(S_p, S_q)$ the choice depends on whether the center of the newly created arc is an element of S_p or S_q . Then the algorithm treats all endpoints of the outgoing edges. If one of the diagrams contains artificial vertices, which do not define the minimal disk, some preprocessing has to be done as such a vertex does not have incoming edges and thus, would otherwise never be processed.

CharacterizeArcDomain(POINTSET S_P, S_Q)

begin

compute L_P - and L_Q -diagram from S_P, S_Q

for every edge e associated with case 12,13 or 14

introduce artificial vertex v on e where minimal distance to e is reached

endifor

for every edge e

assign direction to edge e such that distance to points corresponding to e is increasing

endifor

for every vertex v of type 12 or 13

FollowEdgesFromVertex(v)

endifor

find vertex v_{min} , defining minimal disk

FollowEdgesFromVertex(v_{min})

output characterization

end /* CharacterizeArcDomain */

FollowEdgesFromVertex(VERTEX v)

begin

if all incoming edges of v are labeled

determine case corresponding to v

apply change to $SEQ_r(S)$

choose appropriate diagram

for every outgoing edge e of v

label e

FollowEdgesFromVertex(EndpointOf(e))

endifor

endif

end /* FollowEdgesFromVertex */

Fig. 7. Algorithm for the computation of the characterization of the arc domain of a point set S .

An example characterization of a pattern is given in Table III.

III. SHAPE PARAMETER ESTIMATION

In the previous section the arc domain of a pattern described in parameter space was considered; now we consider the estimation of the radius or curvature from the digital pattern resulting from digitizing a circular arc.

A. The Geometric Minimum Variance Bound

By definition all circular arcs in the arc domain yield the same digital pattern S . However, only one estimate \hat{g} for the shape parameter of the arc can be assigned to the pattern S . As the true shape parameter g varies over different elements in $\mathcal{B}(S)$, an uncertainty is unavoidably introduced in the estimation of the shape parameter of the preimage. This is quantified in the domain variance.

DEFINITION 8. (Domain Variance)

$$VAR_{\hat{g}}(S) = \int_{\omega \in \mathcal{B}(S)} p(\omega / S) (\hat{g}(S) - g(\omega))^2 d\omega,$$

TABLE III

CHARACTERIZATION OF THE ARC DOMAIN OF THE EXAMPLE PATTERN S USED IN FIG. 6. SHOWN ARE THE r -VALUES FOR WHICH CHANGES IN $SEQ_r(S)$ OCCUR. THE POINTS T CAUSING THE CHANGE (WHERE $r = \rho(T)$, THE CASE IN TABLE II CORRESPONDING TO THE CONFIGURATION OF T , AND FINALLY THE CHANGING r -SEQUENCE.

r	T	case	$SEQ_r(S)$
16.8	$\{p_0, p_1, p_2\}$	7	\emptyset ↓
17.0	$\{p_3, p_1, p_0\}$	1	p_0, p_1, p_2 ↓
18.5	$\{p_2, q_1, p_0\}$	8	p_0, p_3, p_2, p_1 ↓
19.7	$\{p_2, p_1, q_2\}$	8	p_0, p_3, q_1, p_2, p_1 ↓
20.2	$\{q_1, p_0, p_3\}$	2	$p_0, p_3, q_1, p_2, q_2, p_1$ ↓
22.5	$\{q_2, p_2, q_1\}$	9	p_0, q_1, p_2, q_2, p_1 ↓
25.5	$\{p_1, p_0, q_2\}$	2	p_0, q_1, q_2, p_1 ↓
31.6	$\{q_1, p_0, q_2\}$	4	p_0, q_1, q_2 ↓ \emptyset

where $p(\omega/S)$ is the probability of ω being the original leading to the pattern S and $g(m, r) = r$ when estimating the radius of the arc and $g(m, r) = 1/r$ for curvature estimation.

We seek the estimator $\hat{g}_{mv}(S)$ minimizing the domain variance, i.e.,

DEFINITION 9.

$$\hat{g}_{mv}(S) = \arg \min_{\hat{g}} \{ \text{VAR}_{\hat{g}}(S) \}$$

This turns out to be the expectation g over the arc domain.

THEOREM 1.

$$\hat{g}_{mv}(S) = \int_{\omega \in \mathcal{B}(S)} p(\omega/S) g(\omega) d\omega$$

PROOF. From the definition of the domain variance and \hat{g}_{mv} we have:

$$\hat{g}_{mv} = \arg \min_{\hat{g}} \left\{ \int_{\omega \in \mathcal{B}(S)} p(\omega/S) (\hat{g} - g(\omega))^2 d\omega \right\}$$

Rewriting the expression, taking constants not depending on ω out of the integration, and using

$$\int_{\omega} p(\omega/S) d\omega = 1$$

yields:

$$\hat{g}_{mv}(S) = \arg \min_{\hat{g}} \left\{ \hat{g}^2 - 2\hat{g} \int_{\omega \in \mathcal{B}(S)} p(\omega/S) g(\omega) d\omega + \int_{\omega \in \mathcal{B}(S)} p(\omega/S) g^2(\omega) d\omega \right\}$$

We are looking for a stationary point with respect to \hat{g} of the above term within the curly braces. Taking the first derivative with respect to \hat{g} and substituting $\hat{g} = \hat{g}_{mv}$ leads to the following condition on $\hat{g}_{mv}(S)$:

$$2\hat{g}_{mv}(S) - 2 \int_{\omega \in \mathcal{B}(S)} p(\omega/S) g(\omega) d\omega = 0$$

The second derivative with respect to \hat{g} of the term within the curly braces is a positive constant (2) not depending on \hat{g} . Hence, the stationary point is a minimum and thus,

$$\hat{g}_{mv}(S) = \int_{\omega \in \mathcal{B}(S)} p(\omega/S) \hat{g}(\omega) d\omega \quad \square$$

As the domain variance is a deterministic measure, the domain variance of \hat{g}_{mv} is the minimal variance one can reach for any possible estimator.² This should be discriminated from the bound on the minimum variance of parameter estimates from stochastic data [5] (MVB, or Cramér-Rao lower bound). In this bound the variance is a stochastic measure. The latter bound is a genuine lower bound only if one restricts the class of estimators to be linear and unbiased. Hence, we define the Geometric variant of the Minimum Variance Bound and denote it by GMVB_g .

DEFINITION 10. (Geometric Minimum Variance Bound)

$$\text{GMVB}_g(S) = \text{VAR}_{\hat{g}_{mv}}(S)$$

The bound quantifies the ability of the pattern S to discriminate among variations in the shape parameter of the preimage of the arc, i.e., it expresses the maximum achievable precision in shape parameter estimation.

To find an expression for the bound we make the following three assumptions:

- 1) Features only depend on r
- 2) There is no preferred position
- 3) Radius and position are independent.

Now, consider the following moment generating function for features g which only depend on r (assumption 1):

$$T_g^i(S) = \int_r \tilde{p}(r/S) g^i(r) dr, \quad (10)$$

where the function $\tilde{p}(r/S)$ is proportional to the conditional probability function on r given the pattern S . It gives the "number" of centers corresponding to this value of r , weighted by the prior probability on r .

The equation has important applications [31]. First, consider $T_g^0(S)$, this gives a measure for the total number of preimages of the pattern. It is the normalization factor needed to make \tilde{p} a proper probability density function. Second, it allows to express g_{mv} and GMVB_g as:

$$\hat{g}_{mv} = \frac{T_g^1(S)}{T_g^0(S)} \quad \text{GMVB}_g(S) = \frac{T_g^2(S)}{T_g^0(S)} - \left(\frac{T_g^1(S)}{T_g^0(S)} \right)^2. \quad (11)$$

In the next section we consider the computation of $T_g^i(S)$.

B. The Computation of the Moment Generating Function

We seek the probability on the radius r , given that the digitization of the arc leads to the digital pattern S . We assume no a priori information on position (assumption 2). Thus, within the domain of S , the centers have a uniform distribution and the probability on r is proportional to the area \mathcal{A} in domain space of the set of arc centers $M_r(S)$. For the time being we leave open the choice for the prior distribution on r . Using the independence of position and radius (assumption 3) we find:

2. In [7] the equivalent theorem for straight lines is proved in a different way. In their proof they need to make the assumption that the estimator is linear. Our result shows that this assumption is not needed.

$$p(r/S) \propto \tilde{p}(r) \mathcal{A}(M_r(S)), \quad (12)$$

and it follows that we have to find an expression for the area of $M_r(S)$.

The boundary of the set $M_r(S)$ is a polygon with curved edges. Let the vertices of $M_r(S)$ be given by \mathbf{v}_i and let ϕ_i be the size of the edge (in radians) connecting \mathbf{v}_i and \mathbf{v}_{i+1} ; then the area of $M_r(S)$ is expressed using dot products as [26]:

$$\mathcal{A}(M_r(S)) = \sum_i \left\{ \frac{1}{2} (\mathbf{v}_i \cdot \mathbf{v}_{i+1})_{\perp} \pm \frac{1}{2} r^2 (\phi_i - \sin \phi_i) \right\} \quad (13)$$

with

$$\begin{pmatrix} x \\ y \end{pmatrix}_{\perp} = \begin{pmatrix} y \\ -x \end{pmatrix}$$

The first term of the equation, summed over all i , gives the area of the straight polygon through the vertices \mathbf{v}_i . The second term corrects for the area of the segment between the curved arc and the chord from \mathbf{v}_i to \mathbf{v}_{i+1} , denoted by $(\mathbf{v}_i, \mathbf{v}_{i+1})$. The area of the segment is added if the curved edge is convex (the center is in S_p) and subtracted if it is concave (the center is in S_q).

We obtain a summation over contributions from individual arcs in the boundary of $M_r(S)$. As noted, each curved edge in $M_r(S)$ is defined by three subsequent points in $\text{SEQ}_r(S)$. Let (s', s, s'') be such a triplet of points and recall that s defines the center and s' and s'' in conjunction with s determine the start and endpoint of the edge.

The start point \mathbf{v}' of the arc lies on the perpendicular bisector of s' and s . To be precise, the start point is an intersection of the circles centered at s' and s with radius r . The two intersections of these circles are given by (see Fig. 8(a)):

$$\mathbf{v}_{s's}(r) = s + \frac{1}{2}(s', s) \pm \frac{\sqrt{r^2 - \frac{1}{4}\|(s', s')\|^2}}{\|(s', s)_{\perp}\|} \quad (14)$$

In [32] it is shown that whenever s, s' are in the same set of S (i.e., $s, s' \in S_p$ or $s, s' \in S_q$) one should take the minus case, otherwise one should take the plus. To find the end point \mathbf{v}'' one simply replaces s' by s and s by s'' .

The size of the arc connecting \mathbf{v}' to \mathbf{v}'' is calculated as:

$$\phi_{s'ss''}(r) = \cos^{-1} \left(\frac{(s, \mathbf{v}_{s's}(r)) \cdot (s, \mathbf{v}_{ss''}(r))}{r^2} \right) \quad (15)$$

The geometric construction used to derive the equation is exemplified in Fig. 8(b).

The contribution \mathcal{A}_r of the triplet (s', s, s'') to the area of the curved polygon $M_r(S)$ is given by:

$$\begin{aligned} \mathcal{A}_r((s', s, s'')) &= \frac{1}{2} \mathbf{v}_{s's}(r) \cdot \mathbf{v}_{ss''}(r)_{\perp} \\ &\pm \frac{1}{2} r^2 (\phi_{s'ss''}(r) - \sin \phi_{s'ss''}(r)) \end{aligned} \quad (16)$$

Now, let $\mathcal{T}(S)$ be the set of all triplets defining edges in the boundary of $M_r(S)$ i.e., all triplets obtained by (cyclically) taking three subsequent points in $\text{SEQ}_r(S)$. Then it follows from (12) that:

$$p(r/S) \propto \tilde{p}(r) \sum_{a \in \mathcal{T}_r(S)} \mathcal{A}_r(a) \quad (17)$$

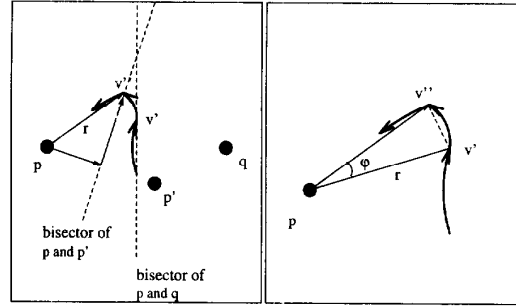


Fig. 8(a). The geometric construct used in (14). The local sequence of edges in the boundary of $M_r(S)$ is given by p', p, q . This triplet defines the curved edge centered at p , starting at \mathbf{v}' and ending at \mathbf{v}'' . The start point \mathbf{v}' is on the perpendicular bisector of p' and p to the left of (p', p) as p' and p are both in S_p . The endpoint \mathbf{v}'' is on the perpendicular of p and q , to the right of (p, q) , as $p \in S_p$ and $q \in S_q$. The vector sum resulting in \mathbf{v}'' is indicated. Any other combination or configuration of points in a triplet defining an edge is treated likewise. (b) The angle ϕ between (p, \mathbf{v}') and (p, \mathbf{v}'') depends on r . It is used in (15) to calculate the area between the straight chord and the curved edge from \mathbf{v}' to \mathbf{v}'' .

Every triplet of points defining an edge in the boundary of $M_r(S)$ does so for a distinct range of r -values, see Section B. Thus, the term under the integral sign in the moment generating function (10) changes (for increasing r) whenever an edge is introduced in the boundary of $M_r(S)$ or one annihilated, i.e., whenever a change to $\text{SEQ}_r(S)$ occurs. It is more convenient to rewrite the equation in terms of the triplets defining edges and their associated minimum and maximum radius. So, let $A(S)$ be the set of all triplets occurring in $\text{SEQ}_r(S)$ for some value of r and let $r_{\min}(a)$ be the value of r at which the edge defined by triplet a occurs in $M_r(S)$ and let r_{\max} be the value at which the edge is annihilated.

We can now summarize the main theoretical result of this paper in the following

THEOREM. 2.

$$T_g^i(S) = \sum_{a \in A(S)} \left(\int_{r_{\min}(a)}^{r_{\max}(a)} \tilde{p}(r) \mathcal{A}_r(a) g^i(r) dr \right),$$

where T_g^i is the moment generating function (10) for the feature g^i (e.g., the radius) to be estimated. $\tilde{p}(r)$ is the a priori distribution of r . $A(S)$ is the set of all triplets of points defining edges in $M_r(S)$ for some value of r and $\mathcal{A}(a)$ is the contribution of triplet a to the area of $M_r(S)$, which is nonzero only for $r \in [r_{\min}(a), r_{\max}(a)]$.

The characterization of the arc domain presented in the preceding section provides us with all the information needed to compute the set $A(S)$ and the associated r_{\min} and r_{\max} values. From there a numerical integration method is used to calculate the moment generation function using Theorem 2. This in turn allows for the computation of the optimal estimator g_m and the GMVB_g using (11).

In Figs. 9 and 10 the lower bound and optimal radius estimate are illustrated for example patterns using a uniform a priori distribution on r .

C. The Positional Error

The Geometric Minimum Variance Bound gives a bound to the precision of the measurement for a given pattern of points. Now consider the estimation of shape properties from a given continuous disk of radius r .

When the continuous disk is placed at some fixed position on the grid and a window containing n Freemancodes is moved along the resulting digital contour, optimal estimates of the radius or curvature will vary for different parts of the contour. Further, when the disk is placed at different positions with respect to the grid, the optimal estimates in the windows vary as the digital contour of the disk is not the same for each position. As the measurement error for a pattern only depends on the codes in the Freemanchain and not on its start position we can fix the start position of all Freemanchains to the origin and see whether it contains arcs of radius r . The expected positional error is thus defined as:

DEFINITION 11. (Positional Error)

$$E_{\hat{g}}^n(r) = \sum_{F^* \in \mathcal{F}^n} p(F^*/r)(g(r) - \hat{g}(F^*))^2$$

As the centers are uniformly distributed we find the following conditional probability for a specific Freemanchain F .

$$p(F/r) = \frac{\mathcal{A}(M_r(F))}{\sum_{F^* \in \mathcal{F}^n} \mathcal{A}(M_r(F^*))} \quad (18)$$

The estimator \hat{g}_{mv} has the smallest expected positional error (for varying r) among all possible estimators:

PROPOSITION 1.

$$\hat{g}_{mv} = \arg \min_{\hat{g}} \left\{ \int_r p(r) E_{\hat{g}}^n(r) dr \right\}$$

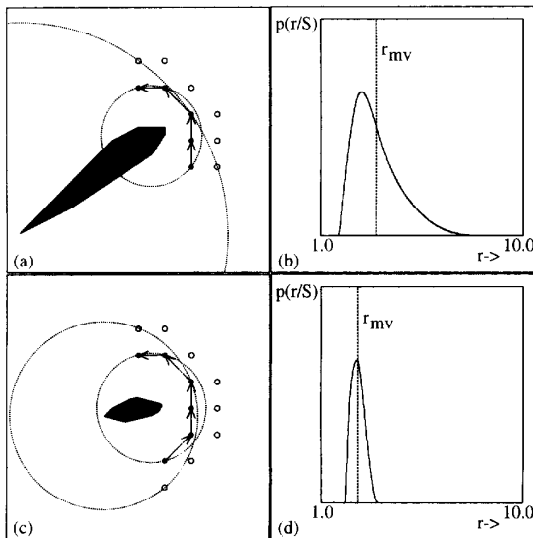


Fig. 9. The example digital pattern S of Fig. 3 with the largest and smallest disk which locally are mapped to the pattern S (a). In (b) the probability on the radius with the optimal radius estimate r_{mv} . Adding one point to pattern S leads to a smaller volume in the arc domain (c). Hence, the radius estimate is more precise (d).

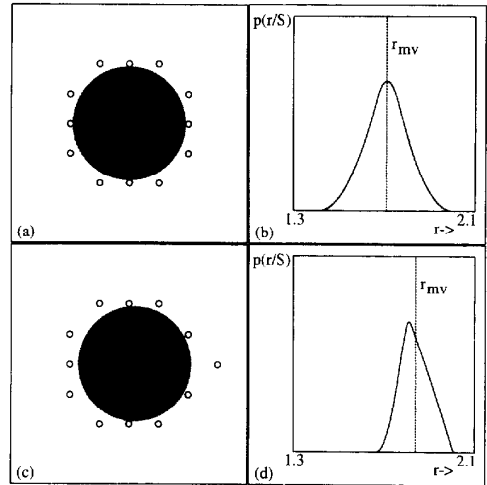


Fig.10. The digitization of the disk with radius 1.9 centered at the origin (a) and the digitization when the disk is positioned at (0.2, 0) (c). Although the preimage of both patterns is equal, different domains are found. Hence, different optimal radius estimates and precisions result (b)(d).

PROOF. From (11) we have:

$$\int_r p(r) E_{\hat{g}}^n(r) dr = \int_r p(r) \left\{ \sum_{F^* \in \mathcal{F}^n} p(F^*/r)(g(r) - \hat{g}(F^*))^2 \right\} dr \quad (19)$$

In order to change the order of integration and summation we apply Bayes' rule to $p(F/r)$ and find:

$$p(F/r) = \frac{p(r/F)p(F)}{p(r)}$$

Let again $\tilde{p}(r)$ denote the unnormalized a priori probability on r . Then the terms in the equation are given by:

$$p(r/F) = \frac{\tilde{p}(r)\mathcal{A}(M_r(F))}{\int_r \tilde{p}(r)\mathcal{A}(M_r(F))dr}$$

$$p(F) \propto \frac{\int_r \tilde{p}(r)\mathcal{A}(M_r(F))dr}{\sum_{F^* \in \mathcal{F}^n} \left\{ \int_r \tilde{p}(r)\mathcal{A}(M_r(F^*))dr \right\}}$$

$$p(r) \propto \tilde{p}(r)$$

Rearranging terms we find:

$$p(F/r) = \frac{\mathcal{A}(M_r(F))}{\sum_{F^* \in \mathcal{F}^n} \left\{ \int_r \tilde{p}(r)\mathcal{A}(M_r(F^*))dr \right\}}$$

By changing the order of summation and integration (noting that the right hand side is a constant times $\mathcal{A}(M_r(F))$) we find:

$$\int_r p(r) E_{\hat{g}}^n(r) dr \propto \sum_{F^* \in \mathcal{F}^n} \left\{ \int_r p(r)\mathcal{A}(M_r(F^*)) (g(r) - \hat{g}(F^*))^2 dr \right\}$$

As we have a sum of positive terms the total expected positional error is minimized if each individual term is minimized. It follows from Theorem 1 that each term is minimized if $\hat{g}_{mv}(F)$ is used which proves the proposition. \square

Hence, the positional error E_g^n for estimator \hat{g}_{mv} quantifies the ultimate bound on the error for shape parameter measurement on the arc when placed at random positions.

To study the error it is convenient to split the error in a bias and a deviation part. The positional bias tells us how the digitization affects the apparent shape of the continuous preimage.

DEFINITION 12. (*Positional Bias*)

$$\text{BIAS}^n(r) = \varepsilon \{ \hat{g}_{mv}(F) \} - g(r)$$

where ε denotes expectation over all elements in \mathcal{F}^n , i.e.,:

$$\varepsilon\{h\} = \sum_{F \in \mathcal{F}^n} p(F/r) h(F).$$

The positional deviation quantifies the ultimate precision with which we can measure the shape parameters of the arc.

DEFINITION 13. (*Positional Deviation*)

$$\text{DEV}^n(r) = \sqrt{\varepsilon \{ \hat{g}_{mv}(F)^2 \} - (\varepsilon \{ \hat{g}_{mv}(F) \})^2}$$

IV. RESULTS

We calculated $\text{BIAS}^n(r)$ and $\text{DEV}^n(r)$ for $n = 7, 8, 9$ with $r \leq \text{MRR}(n)$ for the convex patterns. The results are summarized in Fig. 11, for estimation of the radius of the predigitized arc, and in Fig. 12 for curvature estimation. Both were calculated with uniform priors on the feature to be estimated. They cannot be directly compared as the priors on the radius of the original arcs are different.

From the figures we conclude that the observed radius of the arc increases if we use too few Freeman codes in the chain as confirmed by the curvature estimates obtained. Curvature estimates are unbiased, a consequence of the fact that for curvature estimation the a priori probability on r is proportional to $1/r^2$ and hence favors smaller radii. As expected, more precise estimates are found when n is larger. However, for the range of radii used, the deviation for $n = 9$ is still between 2% and 9% in both radius and curvature estimation. To find better estimates, one needs larger values of n , hence considering larger arcs. As an alternative one can use denser sampling but then one has to change n accordingly to keep the arc in the window of the same size.

Now consider the estimation of the radius r of a disk when given its full digital boundary. Then n is no longer constant but equals the number of points in the digital boundary which varies when the disk is placed at random positions on the grid. The values for bias and deviation are derived from Monte Carlo experiments placing the disk at random position with respect to the grid a 1,000 times. Results are presented in Fig. 13.

It follows that for a full disk the estimation of the radius is virtually unbiased. Deviation is below 1% if the radius is larger than four grid units.

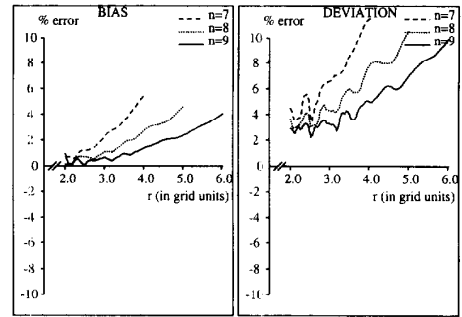


Fig. 11. The $\text{BIAS}^n(r)$ and $\text{DEV}^n(r)$ for radius estimation from (open) circular arcs with r in the range 2.0 to $\text{MRR}(n)$ and $n = 7, 8, 9$. Both expressed as fraction of the true radius.

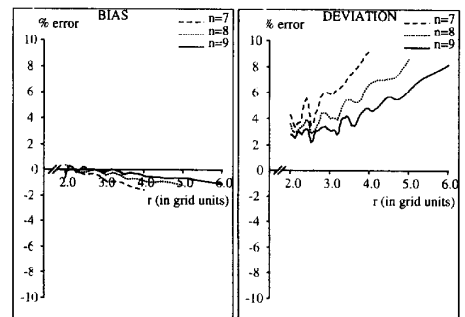


Fig. 12. The $\text{BIAS}^n(r)$ and $\text{DEV}^n(r)$ for curvature estimation from (open) circular arcs with r in the range 2.0 to $\text{MRR}(n)$ and $n = 7, 8, 9$. Expressed as fraction of the true curvature.

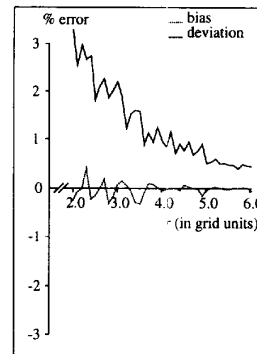


Fig. 13. Optimal estimation of the radius of a full circular disk, when repeatedly placed at random positions with respect to the grid. The bias and deviation are indicated, both relative to the true radius.

V. SUMMARY AND CONCLUSION

In this paper we have considered two topics. First, we have characterized the set of all continuous circular arcs which give rise to a given digitization pattern. Second, we have derived optimal estimates for the curvature and radius of the continuous arc which due to the inherent loss of information in the digitization process cannot be improved.

The local curvature or local radius of an object is estimated by moving a window along the digital contour. Optimal

estimation can only be achieved if all circular arcs which give rise to the specific digital pattern in the window are considered. The set of parameters of arcs which give rise to the pattern is called the arc domain of the pattern.

A domain can be classified as one of six types (straight, strictly convex, infinite convex, strictly concave, infinite concave, and noncircular) which is calculated for all possible Freeman chains of length $n = 3, \dots, 9$ (see Section II.C). Based on the domain types one can find the maximal recognizable radius $MRR(n)$ which poses a limit on the radius of continuous arcs one can estimate using a window of n Freeman codes. The type classification can further be used to decompose a given digital contour of an object into straight, convex, and concave parts. A full characterization of the domain of any specific digital pattern in $(x_{centers}, y_{centers}, radius)$ -space is given in Section II.B based on the changes in the sequence of curved edges bounding the set of centers in the domain for varying r .

The arc domain of a given digital pattern by definition is the set of all predigitized arcs which are mapped to this pattern. As the radius of elements in the arc domain varies, an unavoidable error is made in the radius or curvature estimation. This error is bounded by the equivalent of the Cramér/Rao bound expressing the influence of digitization rather than stochastic noise. It is called the Geometric Minimum Variance Bound (Definition 10). Computation of the GMVB using the characterization of the arc domain is based on the moment generating function given in Theorem 1. The unique estimator achieving this minimal variance is the expectation of the shape feature over the arc domain (Theorem 1). Theorem 2 again provides the basis for computing the estimator in terms of the characterization.

In contrast to methods commonly used (see [34]) the method presented in this paper allows to incorporate prior knowledge on the distribution of the shape parameter of the circular arcs, always achieving optimal precision. The shape of the prior distribution is arbitrary. In the absence of other prior information a uniform distribution of the feature can be assumed (as is used in this paper).

Practical bounds on the precision in measuring curvature or the radius using uniform priors were presented in Section IV. It is found that the relative deviation in the digitization limited optimal shape parameter measurement of arcs placed at random positions with $r \leq 6$ grid units, using a window of $n = 9$ Freeman codes, is between 2% and 9%. For digitizations of full disks (and hence varying n) the deviation is below 1% for $r \geq 4$ grid units.

The bounds derived cannot directly be compared to the more practical curvature measurement methods discussed in [33], [34]. In the reference arcs of larger radii were considered and larger number of Freeman codes were used with a weighting function on the points in the window. However, the presented method does not suffer from any of the problems associated with the other estimators which ignored the two dimensional character of the curve and the special structure of digitized circular arcs. The performance is also better than arc fitting as full knowledge of the digitization process is incorporated. The precision of estimation of the new estimator, even when using small chains, clearly supports these observations.

In practical situations, the theoretical best estimator can be calculated from the digital pattern directly or it can be pre-computed for all patterns of a given size and stored in a lookup table. For chains of nine Freeman codes, the table has about 4,500 entries. All other 33,000,000 chains of nine codes are not the digitization of a circular arc.

This method is particularly useful for problems where some prior knowledge on the distribution of radii is known and where there is a noise-free sampling. It can lead to optimal performance for a given measurement error. For example, in the surveillance of circular holes in industrial objects performance will be critical, the sampling can be arranged such that it is noise-free, and the distribution $p(r)$ is known. Under these circumstances the grid size can be reduced to the bare minimum given the maximum tolerable measurement error.

ACKNOWLEDGMENTS

The remarks made by the reviewers have clearly improved the presentation of the paper. This work was supported by the Dutch Ministry of Economic Affairs through SPIN grants "3D Computer Vision" and "3D Image Analysis."

REFERENCES

- [1] I.M. Anderson and J.C. Bezdek, "Curvature and deflection of discrete arcs: A theory based on the commutator of scatter matrix pairs and its application to vertex detection in planar shape data," *IEEE Trans. Pattern Analysis and Machine Intelligence*, vol. 6, pp. 27-40, 1984.
- [2] H. Asada and M. Brady, "The curvature primal sketch," *IEEE Trans. Pattern Analysis and Machine Intelligence*, vol. 8, no. 1, pp. 2-14, 1986.
- [3] C.A. Berenstein, L.N. Kanal, and D. Lavine, "A geometric approach to subpixel registration accuracy," *Computer Vision, Graphics, and Image Processing*, vol. 40, pp. 334-360, 1987.
- [4] M. Brady and H. Asada, "Smoothed local symmetries and their implementation," *The Int'l J. Robotics Research*, vol. 3, no. 3, pp. 36-60, 1984.
- [5] A. Van den Bos, "Parameter estimation," *Handbook of Measurement Science*, P.H. Sydenham, ed., John Wiley & Sons, 1982.
- [6] L. Dorst and A.W.M. Smeulders, "Discrete representation of straight lines," *IEEE Trans. Pattern Analysis and Machine Intelligence*, vol. 6, pp. 450-463, 1984.
- [7] L. Dorst and A.W.M. Smeulders, "Best linear unbiased estimators for properties of digitized straight lines," *IEEE Trans. Pattern Analysis and Machine Intelligence*, vol. 8, pp. 276-282, 1986.
- [8] L. Dorst and A.W.M. Smeulders, "Length estimators for digitized contours," *Computer Vision, Graphics, and Image Processing*, vol. 40, pp. 311-333, 1987.
- [9] J.S. Duncan, F. Lee, A.W.M. Smeulders, and B.L. Zaret, "A bending energy model for measurement of cardiac shape deformity," *IEEE Trans. Medical Imaging*, vol. 10, no. 3, pp. 307-320, 1991.
- [10] S. Fisk, "Separating point sets by circles, and the recognition of digital disks," *IEEE Trans. Pattern Analysis and Machine Intelligence*, vol. 8, pp. 554-557, 1986.
- [11] H. Freeman, "Boundary encoding and processing," *Picture Processing and Psychopictories*, pp. 241-266. New York: Academic, B.S. Lipkin and A. Rosenfeld, eds., 1970.
- [12] F.C.A. Groen and P.W. Verbeek, "Freeman-code probabilities of object boundary quantized contours," *Computer Graphics and Image Processing*, vol. 7, pp. 391-402, 1977.
- [13] D.I. Havelock, "Geometric precision in noise-free digital images," *IEEE Trans. Pattern Analysis and Machine Intelligence*, vol. 11, no. 10, 1,065-1,075, 1989.

- [14] S.H.Y. Hung, "On the straightness of digital arcs," *IEEE Trans. Pattern Analysis and Machine Intelligence*, vol. 7, no. 2, pp. 203-215, 1985.
- [15] C.E. Kim, Digital disks," *IEEE Trans. Pattern Analysis and Machine Intelligence*, vol. 6, no. 3, pp. 372-374, 1984.
- [16] J. Koplowitz and A.M. Bruckstein, "Design of perimeter estimators for digitized planar shapes," *IEEE Trans. Pattern Analysis and Machine Intelligence*, vol. 11, pp. 611-622, 1989.
- [17] Z. Kulpa, "Area and perimeter measurement of blobs in discrete binary pictures," *Computer Graphics and Image Processing*, vol. 6, pp. 434-454, 1977.
- [18] U.M. Landau, "Estimation of a circular arc center and its radius," *Computer Vision, Graphics and Image Processing*, vol. 38, pp. 317-326, 1987.
- [19] M.D. McLroy, "A note on discrete representation of lines," *AT&T Technical J.*, vol. 64, no. 2, pp. 481-490, 1985.
- [20] F. Mokhtarian and A. Mackworth, "Scale-based description and recognition of planar curves and two-dimensional shapes," *IEEE Trans. Pattern Analysis and Machine Intelligence*, vol. 8, no. 1, pp. 34-43, 1986.
- [21] A. Nakamura and K. Aizawa, "Digital circles," *Computer Vision, Graphics, and Image Processing*, vol. 26, pp. 242-255, 1984.
- [22] J. O'Rourke, S.R. Kosaraju, and N. Medgiddo, "Computing circular separability," *Discrete and Computational Geometry*, vol. 1, pp. 105-113, 1986.
- [23] F.P. Preparata and M.I. Shamos, *Computational Geometry, an Introduction*. Springer Verlag, 1985.
- [24] D. Proffitt and D. Rosen, "Metrication errors and coding efficiency of chain-encoding schemes for the representation of lines and edges," *Computer Graphics and Image Processing*, vol. 10, pp. 318-332, 1979.
- [25] A. Rosenfeld and A.C. Kak, *Digital Picture Processing*. Academic Press, 2nd ed., 1982.
- [26] S.M. Selby, *Standard Mathematical Tables*. CRC Press, 1975.
- [27] S.W.M. Smeulders and M. Worrington, "Accurate measurement of shape at low resolution," *Pattern Recognition and Artificial Intelligence*. L.N. Kanal and E.S. Gelsema, eds., vol. 7, *Machine Intelligence and Pattern Recognition*, pp. 91-102. North-Holland, 1988.
- [28] D.J. Struik, *Lectures on Classical Differential Geometry*. New York: Dover Publications, Inc., 1984.
- [29] S.M. Thomas and Y.T. Chan, "A simple approach for the estimation of circular arc center and its radius," *Computer Vision, Graphics, and Image Processing*, vol. 45, 1989.
- [30] A.M. Vosepoel, "Estimating the size of circular pre-images from coarsely digitized representations," *Proc. ICPR: Image, Speech and Signal, Analysis*, The Hague, 1992.
- [31] A.M. Vosepoel and A.W.M. Smeulders, "Vector code probability and metrication error in the representation of straight lines of finite length," *Computer Graphics and Image Processing*, vol. 10, pp. 347-364, 1982.
- [32] M. Worrington, "Shape analysis of digital curves," PhD thesis, Univ. of Amsterdam, 1993.
- [33] M. Worrington and A.W.M. Smeulders, "The accuracy and precision of curvature estimation methods," *Proc. ICPR: Image, Speech and Signal, Analysis*, The Hague, 1992.
- [34] M. Worrington and A.W.M. Smeulders, "Digital curvature estimation," *CVGIP: Image Understanding*, vol. 58, no. 3, pp. 366-382,, 1993.



Marcel Worrington received his MSc degree (honors) in computer science in 1988 from the Free University Amsterdam. In 1993 he received his PhD degree at the University of Amsterdam, for a thesis on "The accurate measurement of properties from digital images and its applications in biological and medical imaging." Part of his PhD research was performed at Yale University in the Department of Diagnostic Imaging. Currently, he holds a postdoctoral position at the University of Amsterdam on document image analysis and model based video analysis.



Arnold W.M. Smeulders is professor of computer science on multimedia information systems, and professor of biology on 3D microscopical imaging.

A.W.M. Smeulders has been in image processing since 1977 when he completed his MSc in physics from Delft University of Technology.

Initially, he was interested in accurate and precise measurement from digital images. His current interest is in image databases and intelligent interactive image analysis systems, as well as method and system engineering aspects of image processing and image processing for documents and geographical information.

cal information.